Aerodynamic Contrails: Phenomenology and Flow Physics

K. GIERENS, B. KÄRCHER, H. MANNSTEIN, AND B. MAYER

Deutsches Zentrum für Luft- und Raumfahrt (DLR), Institut für Physik der Atmosphäre, Oberpfaffenhofen, Germany

(Manuscript received 20 February 2008, in final form 9 July 2008)

ABSTRACT

Aerodynamic contrails have been recognized for a long time although they appear sporadically. Usually one observes them under humid conditions near the ground, where they are short-lived phenomena. Aerodynamic contrails appear also at cruise levels where they may persist when the ambient atmosphere is ice-supersaturated. The present paper presents a theoretical investigation of aerodynamic contrails in the upper troposphere. The required flow physics are explained and applied to a case study. Results show that the flow over aircraft wings leads to large variations of pressure and temperature. Average pressure differences between the upper and lower sides of a wing are on the order of 50 hPa, which is a quite substantial fraction of cruise-level atmospheric pressures. Adiabatic cooling exceeds 20 K about 2 m above the wing in a case study shown here. Accordingly, extremely high supersaturations (exceeding 1000%) occur for a fraction of a second. The potential consequences for the ice microphysics are discussed. Because aerodynamic contrails are independent of the formation conditions of jet contrails, they form an additional class of contrails that might be complementary because they form predominantly in layers that are too warm for jet contrail formation.

1. Introduction

The most obvious effect of aviation in the atmosphere is the production of condensation trails (contrails). The contrails that one often observes in the upper troposphere (cruise altitudes of international flights, 8–13 km) are produced from the water vapor in the exhaust gas and from the exhaust particles that serve as condensation nuclei when the mixing of the hot and moist exhaust gases with the cold and dry ambient air leads temporarily to a state of water saturation in the mixture. Liquid droplets form and quickly freeze because of the low temperatures in the upper troposphere. The condition that water saturation (instead of ice saturation) must be reached for contrail formation is known as the Schmidt–Appleman criterion (Schmidt 1941; Appleman 1953). A complete derivation of that criterion has been given by Schumann (1996). Because contrails, when they are produced in ice-supersaturated air, persist and spread in a sheared wind field, they sometimes lead to extended decks of ice clouds (Kuhn 1970; Schumann 1994; Minnis et al. 1998), called contrail cirrus. There is concern that contrail cirrus contribute to climatic warming; hence, contrails and contrail cirrus are a matter of intense research (Boucher 1999; Penner et al. 1999; Zerefos et al. 2003; Mannstein and Schumann 2005; Stordal et al. 2005; Stubenrauch and Schumann 2005).

Exhaust contrails are not the only form of condensation that aircraft can trigger. Condensation can generally occur in accelerated air flows when the temperature drops locally due to conservation of energy in (nearly) adiabatic conditions (Bernoulli's law). Near the ground and under relatively humid (but subsaturated) conditions, one can often observe the formation of short-lived clouds originating from vortices, lift, and transonic flows. Vortex- and lift-generated condensation is supported by high-g maneuvers of the aircraft (i.e., strong acceleration) to accelerate the flow sufficiently for a strong cooling effect. Strong vortical flow acceleration occurs at wingtips and flaps and other sharp corners and edges, as well as at the tips of propeller blades of both airplanes and helicopters. These bodies exert forces on the moving air, which implies vortex generation via the Kutta–Joukowski law (e.g., Landau and Lifshitz 1987, or any other textbook on fluid dynamics). The pressure (and temperature) drop within the vortex tubes can lead to condensation. Such phenomena also occur when flying

Corresponding author address: Klaus Gierens, Institut für Physik der Atmosphäre, DLR Oberpfaffenhofen, Wessling D-82234, Germany.
E-mail: klaus.gierens@dlr.de

DOI: 10.1175/2008JAS2767.1

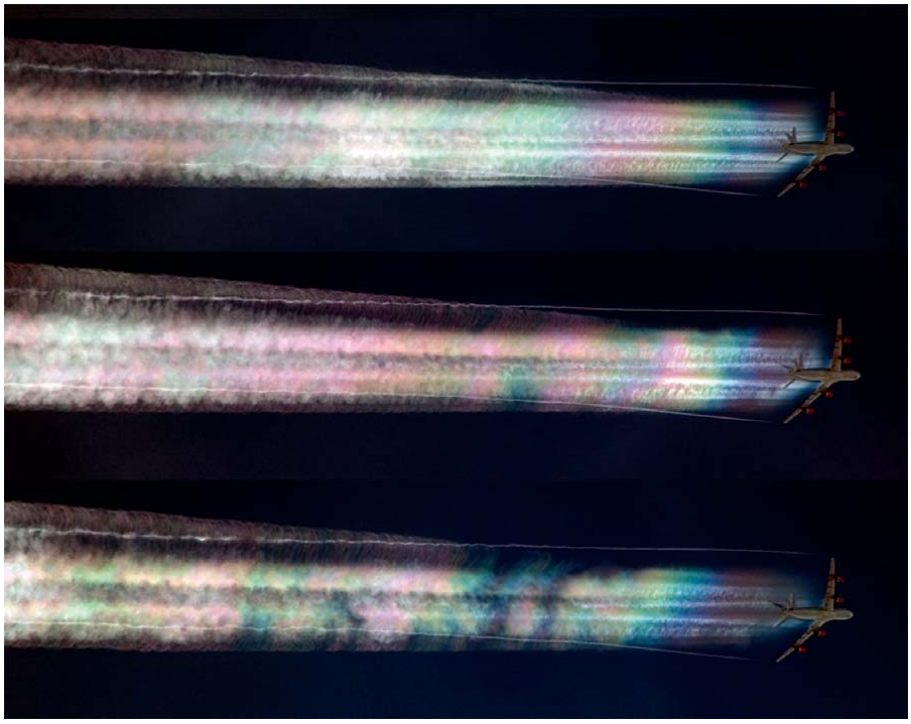

FIG. 1. Composite photographs of aerodynamically induced condensation during cruise-level flight. Note the iridescent colors. Condensation also occurs in thin vortex tubes at the wing tips. Exhaust jet contrails would form at about the position of the tail wing; obviously they do not form in this case. The photograph is reproduced with permission from the photographer Jeff Well.

through supercooled clouds; here the aerodynamic effects cause the so-called aircraft-produced ice particles (APIP) mechanism (Rangno and Hobbs 1983, 1984; Vonnegut 1986; Sassen 1991). Condensation in transonic flows (i.e., subsonic flow becomes supersonic over the wing and other upward curved surfaces, such as the pilot canopy) is called Prandtl–Glauert condensation; this yields the famous cone-shaped clouds that have a sharp rear surface due to the shock front that reverses the supersonic into a subsonic flow. Aerodynamic contrails of these kinds have been discussed by the military for a long time (e.g., they are mentioned in Rhode and Pearson 1942). Although many photographs can be found on the Internet (search on key words ''aircraft, condensation'' or see examples on www.airliners.net), they seem to occur sporadically because they require humid conditions combined with high speed and wing loading.

At higher altitudes under sufficiently cold conditions, the droplets that form in the condensation event may survive after the passage of the aircraft when the ambient air is (super)saturated with respect to ice. Droplets, once frozen, will then be stable in ice-saturated air or even grow in supersaturated air. In this paper and the companion paper (Kärcher et al. 2009), we investigate aerodynamic condensation and freezing generated by the lifting surface of aircraft under cold and ice-saturated conditions typical of the upper troposphere. Under favorable conditions for ice crystal growth and with appropriate illumination of the scene from the sun, beautiful iridescent effects can appear, as shown in Fig. 1. The figure shows clearly that the condensation starts right over the wing and is decoupled from the engine exhaust. The aerodynamic condensation does not originate over the full wing span but is confined to the inner part where wing depth and thickness are largest. The ice crystals survive at least throughout the period seen in the photograph, and the iridescence implies that their size was comparable to the wavelength of visible light, which requires at least ice-saturated conditions. However, the clear sky indicates that the humidity was not sufficient for ice crystals to form naturally. An exhaust contrail, if it had been formed in the shown scene, would be visible from about the tail plane onwards. Its absence proves that the Schmidt–Appleman criterion was not fulfilled. In this case it was too warm (241 K).

The present paper provides the aerodynamic details of the flow perturbation by the wing, including the effect on pressures, temperatures, and relative humidity; in Kärcher et al. (2009) we use these results to simulate the formation process and the microphysical and optical evolution of the formed particles. The outline of this

paper is as follows: In section 2 we give a simple argument as to why this kind of condensation should be expected, and we present our method of calculation of an idealized compressible flow field around a generic wing profile. This method is applied to a case study in section 3. In section 4 we discuss visibility issues and the importance of the phenomenon. The final section 5 gives a summary of the results and presents our conclusions.

2. Aerodynamics

a. Simple calculation

Let us begin with a very simple ''back of the envelope'' reckoning. The difference in average pressure above and below the wings generates the force that carries the aircraft. Let the aircraft weight be W and its wing area A: then the pressure difference is $\Delta p = -W/A$. For wide-body aircraft (e.g., A340, B747), this amounts to a value of typically -50 hPa, a large value in meteorological terms. Now assume that this pressure difference arises adiabatically in the flow. Then the corresponding temperature difference is given by $\Delta T/T = [(\gamma - 1)/\gamma](\Delta p/p)$, with $\gamma = c_p/c_V = 1.4$ being the ratio of the specific heats of air. For near-ground conditions we get approximately $\Delta T = -5$ K, but for typical conditions at cruise altitudes (e.g., $T = 220$ K, $p = 220$ hPa) we get $\Delta T = -14$ K—that is, a sudden cooling above the wing that suffices to turn even relatively dry air of, say, $\mathrm{RH}_i = 20\%$ transiently into a supersaturated state, thus enabling condensation. From this rough calculation we see that aerodynamically induced condensation should be a usual phenomenon under upper tropospheric conditions, and the question arises of why one is rarely able to observe it. To answer this and other questions we have to perform more detailed flow calculations.

b. Generic wing profile

In the following we assume that the flow is adiabatic and circulation-free and furthermore that the flow is strictly two-dimensional and stationary as well as inviscid. First we need to define the shape of the airfoil (i.e., the cross section of the wing). For our goal of providing a first analysis of aerodynamic contrails in the context of aviation effects on the atmosphere, it is sufficient to use a simple but realistic shape and to neglect technical details. For further detailed investigations, in particular when boundary layer effects are considered, one has to turn to more advanced computational fluid dynamics codes, which then allows us also to treat actually used wing profiles.

We have chosen a simple analytical yet realistic shape, a so-called Joukowski wing. This shape results from a conformal mapping of a unit circle, which is very convenient. Let $z = x + iy$ be any complex number, and let $z_c = x_c + iy_c$ be the center of the unit circle, $|z_c| < 1$, and $y_c \geq 0$. Let $\lambda = \sqrt{1 - y_c^2} - x_c$. Then the Joukowski transformation

$$z' = z + \lambda^2/z,$$

when applied to all points z on the unit circle around z_c, yields a curve that is the cross section through a wing. In particular it has one sharp (trailing) and one round (leading) edge. The real and imaginary parts of z_c determine the thickness and camber of the wing, respectively. After application of the Joukowski transformation, the coordinates are multiplied by a constant and shifted to obtain a wing with a leading edge at $x' = 0$ and a trailing edge at $x' = 1$ (In the following we omit the primes). More realistic dimensions are introduced only at the end by use of a scaling factor. Figure 2 shows the geometry of the Joukowski wing.

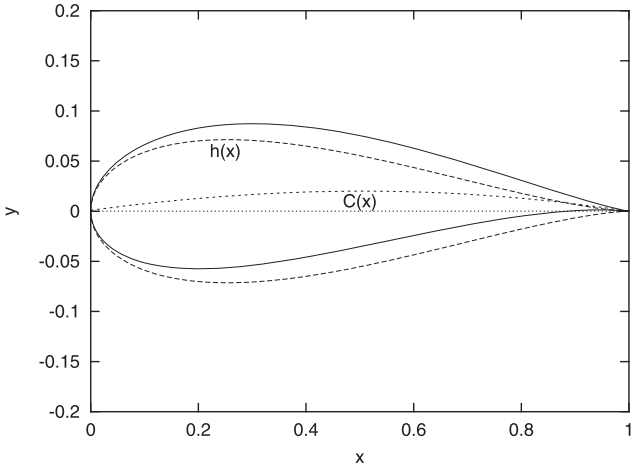

FIG. 2. Geometry of a Joukowski airfoil with $x_c = 0.11$, $y_c = 0.04$. The solid line is the wing surface. The surface can mathematically be represented as the sum of the surface of a symmetric wing (long dashed) plus a camber curve $C(x)$ (short dashed); $h(x)$ is the upper surface of the symmetric wing. Note that the y axis has been expanded for easier viewing.

Given an incompressible flow, we could now compute the velocity potential and streamfunctions for the Joukowski wing simply from the corresponding quantities in a flow around a circular cylinder. The analytical form of the latter is known, and applying the same conformal mapping to these fields as to the wing shape (i.e., the Joukowski transformation) yields the desired result. However, flow incompressibility requires flow speeds with small Mach numbers ($\mathrm{Ma} \ll 1$), whereas modern airliners typically cruise at $\mathrm{Ma} = 0.8$. Therefore, we cannot assume that the flow is incompressible, and we need another method of computation.

c. Compressible flow

1) METHOD OF SINGULARITIES

The following derivations follow the representation in chapter 6 of Zierep (1976). Under the stipulated assumptions, the continuity and Euler equations combine to the following equation for the flow potential:

$$\left(1-\frac{\Phi_x^2}{c^2}\right)\Phi_{xx}+\left(1-\frac{\Phi_y^2}{c^2}\right)\Phi_{yy}-\frac{2\Phi_x\Phi_y}{c^2}\Phi_{xy}=0.$$

Here, c is the speed of sound, and $\Phi_{xy}=\partial^2\Phi/\partial x\partial y$ and so on for the other partial derivatives; Φ is the flow potential, that is, the two components of the velocity vector are $u=\Phi_x$ and $v=\Phi_y$. [Note that in the incompressible case (i.e., $c\to\infty$) we retain the classical (Laplace) potential equation $\Phi_{xx}+\Phi_{yy}=0$.]

Now we make the additional assumption that the parallel background flow (u_0, v_0) is only weakly perturbed by the wing. The background flow is assumed to have a small angle of attack α relative to the wing, so that $(u_0, v_0)=(U_0\cos\alpha, U_0\sin\alpha)$ with the upstream wind speed $U_0=\sqrt{u_0^2+v_0^2}$. With these assumptions, we linearize the potential equation; that is, we neglect perturbation terms of at least quadratic order. Then perturbations caused by the thickness of the wing and by its camber are separable and can simply be superimposed. Because every wing shape can be viewed as a sum of a symmetric shape plus a camber line with zero thickness, we make the following approach for the potential:

$$\Phi(x,y)=\phi_1+\phi_2$$

with

$$\phi_1(x,y)=u_0x+\phi(x,y)\quad\text{and}$$
$$\phi_2(x,y)=v_0y+\bar{\phi}(x,y). \tag{1}$$

Here, ϕ_1 is a potential for a flow around the symmetric airfoil with zero angle of attack, while ϕ_2 is the flow around a thin cambered plate (we also take into account that the angle of attack is nonzero by having $v_0\neq 0$). With this ansatz we get the following potential equations when we only carry on terms that are linear in the perturbation quantities $\phi, \bar{\phi}, \alpha$, and v_0:

$$(1-\mathrm{Ma}^2)\phi_{xx}+\phi_{yy}=0,$$

and the corresponding equation for $\bar{\phi}$. The Mach number for the background flow is $\mathrm{Ma}=U_0/c_0$. It can be noted that a simple coordinate transformation, $x=\xi$ and $\beta y=\eta$, with the abbreviation $\beta=\sqrt{1-\mathrm{Ma}^2}$, again yields the Laplace equation $\phi_{\xi\xi}+\phi_{\eta\eta}=0$. Because this transformation is not a conformal mapping, the simple technique mentioned above for incompressible flows does not work in the more general case. Therefore, we solve the Laplace equation using a method that is known as the method of singularities (Zierep 1976).

In the method of singularities the flow potential is generated by a suitable superposition of two distinct types of singular potentials, one representing the potential of a single point source at (ξ, η), namely,

$$\varphi(x,y)=m(\xi,\eta)\log\sqrt{(x-\xi)^2+\beta^2(y-\eta)^2},$$

where $m>0$ is the source strength (or $m<0$ the sink strength), and the other yielding a singular vortex at (ξ, η), namely,

$$\bar{\varphi}(x,y)=n(\xi,\eta)\arctan\left(\beta\frac{y-\eta}{x-\xi}\right)$$

with vorticity n. (Note that a superposition of singular vortices does not contradict the assumption that the flow is free of circulation; the circulation around every closed path in the flow that does not enclose any singular vortex has zero circulation.)

2) SYMMETRIC WING PROFILE

We assume that the symmetric part of our wing is slim, so that in formulating the boundary conditions on the wing surface we can let $y\to 0$. It is then clear from the symmetry of the problem that the singular sources and sinks have to be placed along the x axis inside the wing, such that

$$\phi(x,y)=\frac{1}{\pi\beta}\int_0^1 m(\xi)\log\sqrt{(x-\xi)^2+\beta^2(y-\eta)^2}\,d\xi.$$

The prefactor serves normalization. The source and sink strengths follow from application of the boundary condition (the flow follows the contour of the wing), giving

$$m(x)=u_0h'(x),$$

where $h(x)$ represents the contour of the symmetric wing (see Fig. 2) and h' is its slope. As mentioned before, the leading edge of the Joukowski wing is round (as it is for every practical wing), such that the slope is infinite at that point. At this point our assumption of a slim wing is not fulfilled, which causes a logarithmic singularity that is typical of linearized calculations of subsonic flows. Fortunately, the singularity is benign

for the later computation of trajectories. Inserting the equation for $m(x)$ into the superposition for $\phi(x, y)$ and differentiating gives the flow field around a slim symmetric wing with zero attack angle:

$$u - u_0 = \frac{1}{\pi\beta}\int_0^1 \frac{u_0 h'(\xi)\,(x-\xi)}{(x-\xi)^2+\beta^2 y^2}\,d\xi$$
$$v = \frac{1}{\pi}\int_0^1 \frac{u_0 h'(\xi)\beta y}{(x-\xi)^2+\beta^2 y^2}\,d\xi. \qquad (2)$$

3) Effect of camber and angle of attack

The calculation of the camber effect follows the same strategy; that is, we generate $\bar{\phi}$ by a suitable superposition of singular vortices, arranged on the x axis between 0 and 1:

$$\bar{\phi}(x, y) = \frac{1}{2\pi}\int_0^1 n(\xi)\,\arctan\left(\beta\frac{y}{x-\xi}\right)\,d\xi.$$

The vortex strength at $(x, 0)$ is computed from the boundary conditions, which express the fact that the local vorticity is given by the jump of the u velocity from below to above the wing; that is,

$$n(x) = u_{\text{below}}(x, 0) - u_{\text{above}}(x, 0) = 2[u_0 - u_{\text{above}}(x, 0)].$$

Differentiation now results in an integral equation for the flow components (a so-called Betz integral equation). From its infinite set of possible solutions we choose the one that renders the flow finite at the trailing edge (fulfilling the Kutta–Joukowski condition). This gives then the following equation for the vorticity distribution (for details, see Zierep 1976):

$$n(x) = -2u_0\sqrt{\frac{1-x}{x}}\left[\frac{\alpha}{\beta} - \frac{1}{\pi\beta}\int_0^1 \frac{C'(x)}{\xi - x}\sqrt{\frac{\xi}{1-\xi}}\,d\xi\right],$$

where $C'(x)$ is the slope of the camber line of the wing (see Fig. 2) and α is the angle of attack in radians. The expression for the singular vorticities can then be used in the following equations for the flow disturbances due to the camber:

$$\bar{u} - u_0 = \frac{-1}{2\pi}\int_0^1 \frac{n(\xi)\beta y}{(x-\xi)^2+\beta^2 y^2}\,d\xi$$
$$\bar{v} - v_0 = \frac{1}{2\pi\beta}\int_0^1 \frac{n(\xi)\,(x-\xi)}{(x-\xi)^2+\beta^2 y^2}\,d\xi. \qquad (3)$$

The superposition of the two flow fields for the symmetric wing and the cambered plate yields the desired solution. The resulting lift F can be computed from the Kutta–Joukowski law, $F = |\Gamma|\rho u_0 \pi B/4$, where Γ is the circulation around the wing contour, which can be computed by integrating the single vorticities [$\Gamma = \int_0^1 n(x)\,dx$], ρ is the density of the air, B is wing span, and the factor $\pi/4$ accounts for the usual elliptic loading of the wing. There is a certain angle of attack α_0 at which the uplift is zero. The effective angle of attack has to be computed from that α_0 upward. In our calculation we use an effective attack angle of 1°. The attack angle at zero uplift is about 0.8°.

d. Trajectory calculation

From the flow field $\mathbf{u}(\mathbf{x})$, we computed a set of trajectories $\mathbf{x}(t)$ both below and above the wing, all initialized at a distance of 50 m in front of the wing ($\mathbf{x}_0$):

$$\mathbf{x}(t) = \mathbf{x}_0 + \int_0^t \mathbf{u}[\mathbf{x}(t')]dt'.$$

The trajectories are computed using a fourth-order Runge–Kutta scheme (Press et al. 1989). The perturbation of the (dominating) x component of the flow speed on the trajectories, $u+\bar{u}-2u_0$, is then inserted into a generalized Bernoulli equation to yield the temperatures along the trajectories; that is,

$$T = T_0 - \frac{\gamma - 1}{2\gamma R_a}\left[(u + \bar{u} - u_0)^2 - u_0^2\right],$$

where R_a is the specific gas constant of air (287 J kg^{-1} K^{-1}). The corresponding pressure is obtained from the Poisson equation:

$$p = p_0\left(\frac{T}{T_0}\right)^{\frac{\gamma}{\gamma-1}}.$$

Similarly, we compute the saturation ratio (with respect to ice) S_i along the trajectories:

$$S_i = \frac{q_{i0}p}{e_i^*},$$

where q_{i0} is the vapor volume mixing ratio in the environment and e_i^* is the saturation vapor pressure over ice (Marti and Mauersberger 1993).

3. Case study

The aircraft shown in Fig. 1 producing an aerodynamic contrail is an A340 with a wingspan of about 60 m. The wing chord (i.e., the depth of the wing directly at the fuselage) is about 11.7 m and the root thickness about 1.7 m. It flew at 9600-m altitude and the photograph was taken out of the cockpit of another aircraft flying at 8400-m altitude (i.e., at a vertical distance of 1200 m). The aerodynamical triggering of condensation is strongest

close to the fuselage, so we treat that case first. From weather analyses of the National Centers for Environmental Prediction (NCEP) we obtain an ambient pressure of 300 hPa and an ambient temperature 241 K, and we assume a flight speed of Ma = 0.8 and an effective angle of attack of 1°. Streamlines for this case, as well as pressure, temperature, and saturation ratio histories along these streamlines, are presented in Figs. 3–6. The slim wing approximation is justified when the thickness parameter (here 1.7/11.7 = 0.14) is small. The relative error in the flow field calculation is on the order of the square of the thickness parameter (Zierep 1976, p. 140), in our case on the order of 0.02, which we consider acceptable.

Looking first at the pressure histories of Fig. 4, we note that the pressure is lower than in ambient air both above and below the wing as a consequence of the flow acceleration on both sides of the wing profile. The pressure drop is, of course, larger above than below the wing, which results in the uplift that carries the aircraft. The pressures are higher than in ambient air at both the front and the rear stagnation points. At the front stagnation point it is simply the obstacle posed by the wing in the airflow that causes the pressure to rise. At the rear stagnation point it is the deceleration of the airflow that leads to the pressure increase before it relaxes to ambient values further downstream. Trajectories that come close to the wing experience stronger pressure effects than trajectories further away. The thickness of the laminar boundary layer is on the order of $\sqrt{\eta L/\rho_0 U_0}$ [Landau and Lifshitz 1987, Eqs. (39) and (12)], with wing depth L, ambient air density ρ_0, and air viscosity $\eta = 1.57 \times 10^{-5}$ N s^{-1} m^{-2}, which is a few millimeters. The thickness of the subsequent turbulent boundary layer is on the order of $x\sqrt{c}$ [Landau and Lifshitz 1987, Eqs. (44) and (6)], with the drag factor

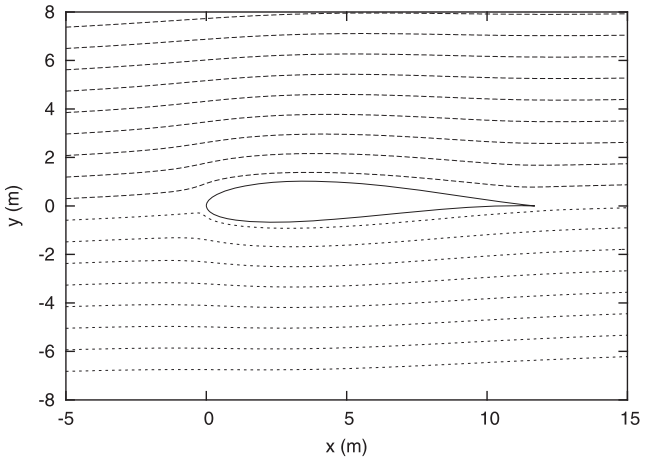

FIG. 3. Trajectories (streamlines) of the airflow around a Joukowski wing of 11.70-m depth and 1.70-m thickness. The flow Mach number is 0.8, and the effective angle of attack is 1°.

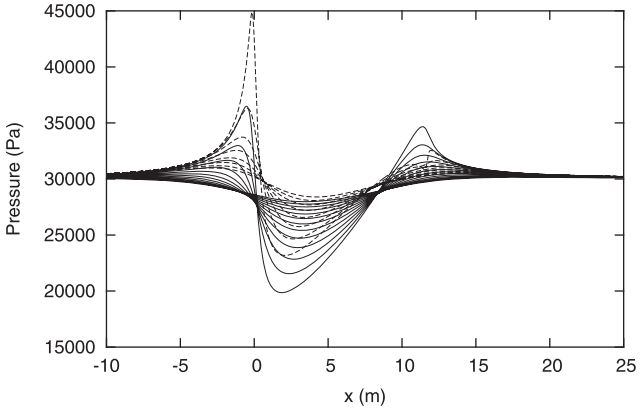

FIG. 4. Pressure variation on the trajectories of Fig. 3. Solid lines correspond to trajectories above the wing; dashed lines refer to trajectories below the wing. The vertical distance of the streamlines in the undisturbed farfield is about 60 cm. Note that the pressure drop is stronger above than below the wing. The resulting upward force carries the aircraft. Ambient pressure is 300 hPa.

$c \approx 0.002$; the maximum estimate ($x = L$) of this is about 45 cm. Hence, neglecting boundary layer effects in our method was justified and all streamlines we have computed (Fig. 3) are above the boundary layer. In the case shown here, the streamlines that are about one wing depth away from the wing profile are only marginally affected by the wing; hence the wing depth is a good length scale for the discussions that follow in Kärcher et al. (2009). The histories of temperature and saturation ratio shown in Figs. 5 and 6 are qualitatively similar to the pressure histories; that is, the front and rear stagnation points cause higher temperatures and lower saturation ratios than in the ambient atmosphere, whereas in the accelerated air above and below the wing the temperature is lower and the saturation ratio is higher. It is noteworthy that the temperature drop above the wing reaches values of more than 20 K in the investigated case. Closer than about 2 m to the wing

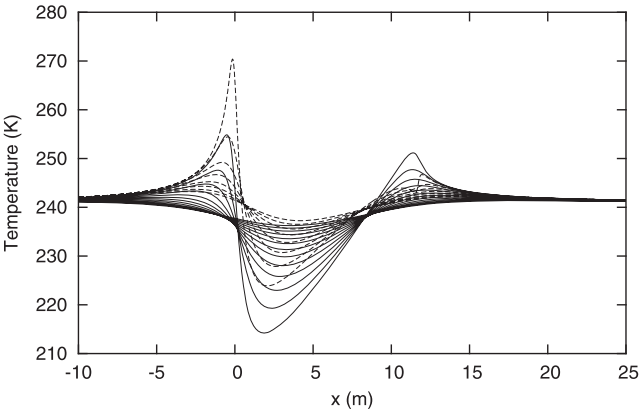

FIG. 5. As in Fig. 4, but for the temperatures. Ambient temperature is 241 K.

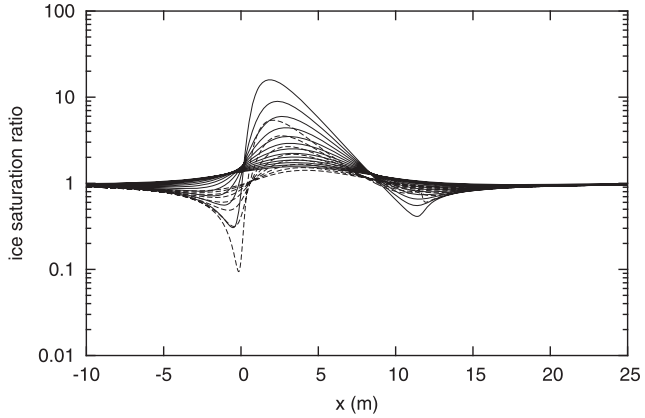

FIG. 6. As in Fig. 4, but for the ice saturation ratio. Ambient saturation ratio is 1.

surface the temperature drop is even larger. Accordingly, the saturation ratio increases by factors exceeding 10; thus, the relative humidity in the airflow over a wing reaches extremely high values that do not occur elsewhere in the troposphere. The temperature minimum and supersaturation maximum are reached within a few milliseconds; that is, the cooling rate obtains extremely high values as well, which has exceptional consequences for the microphysics in the airflow, as shown in Kärcher et al. (2009).

The images show condensation preferably on the inner parts of the wings where the wing is thickest and its depth is largest. There is no condensation in the outer parts of the wing where it is thinner and less deep. We have performed a similar flow calculation for a wing with 6-m depth and about 90-cm thickness (simply a scaled version of the thicker wing discussed above). The airflow is a scaled version of the one described above as well. We find that the maximum pressure perturbation for the upper streamlines decreases roughly in an exponential way with vertical distance from the wing: the *e*-folding scale is half the wing depth; that is,

$$ {}_m\Delta p(y) \approx {}_m\Delta p(0)\, \exp(-2y/L), $$

where ${}_m\Delta$ designates the maximum perturbation along a trajectory. [The expression ${}_m\Delta p(0)$ is not meant to imply that there is a trajectory at $y = 0$.] The maximum temperature perturbation scales accordingly, involving the Poisson law:

$$ {}_m\Delta T(y) = T_0 \left\{ \left[\frac{p_0 + {}_m\Delta p(y)}{p_0} \right]^{(\gamma-1)/\gamma} - 1 \right\}. $$

Both ${}_m\Delta p(y)$ and ${}_m\Delta T(y)$ are negative above the wing. The maximum supersaturation along the trajectories follows from

$$ \max[S(y)] = S_0 \frac{p_0 + {}_m\Delta p(y)}{p_0} \frac{e_i^*(T_0)}{e_i^*[T_0 + {}_m\Delta T(y)]}. $$

Very high supersaturation is reached over a shorter wing depth, too, but it occurs closer to the wing surface and, of course, for a smaller distance along the wing. The maximum excess water vapor concentration over the wing is

$$ \max[W(y)] = \{\max[S(y)] - 1\} \frac{e_i^*[T_0 + {}_m\Delta T(y)]}{R_v[T_0 + {}_m\Delta T(y)]}. $$

The maximum of this function does not occur directly above the wing (where the maximum supersaturation is reached); instead, it is found about 1 m above the wing for the 6-m depth case and about 2.5 m above the wing for 11.7-m depth. The integral $\int \max[W(y)]dy$ turns out to be approximately proportional to the wing depth in the two cases considered here. This integral represents a maximum achievable ice water path (if all excess water could immediately turn into ice). Hence, the visibility (the optical thickness) of the condensation phenomenon scales to first order with the wing depth. Second-order effects arise from the fact that microphysical processes have less time to work at the outer parts of a wing than at the inner parts. This explains why the condensation is invisible in the outer parts of the wing.

4. Discussion

The airflow around an airfoil experiences cooling both on the upper and the lower surface. Although the cooling on the upper side is stronger, it is still substantial on the lower side (more than 10 K in Fig. 5). Accordingly, the relative humidity can reach quite high values there, too, which should allow condensation. But the images and photographs we have looked at do not show signs of condensation in the airflow underneath the wing, which requires an explanation. Figure 7 shows the supersaturation history for a pair of streamlines that encounter the wing symmetrically, 45 cm below and 45 cm above the leading edge. The heating and drying in the approach of the stagnation point is very similar, so the aerosol in the airflow experiences similar microphysical effects before it encounters the wing. Then, however, the supersaturation reaches much larger values above the wing than below the wing. Nevertheless, the supersaturation below the wing reaches quite high values that are otherwise not present in the troposphere; hence, there is probably condensation in the flow below the wing, too, albeit substantially less than above the wing. As the images show, aerodynamic contrails are translucent (optically thin). Aerodynamic contrails from the

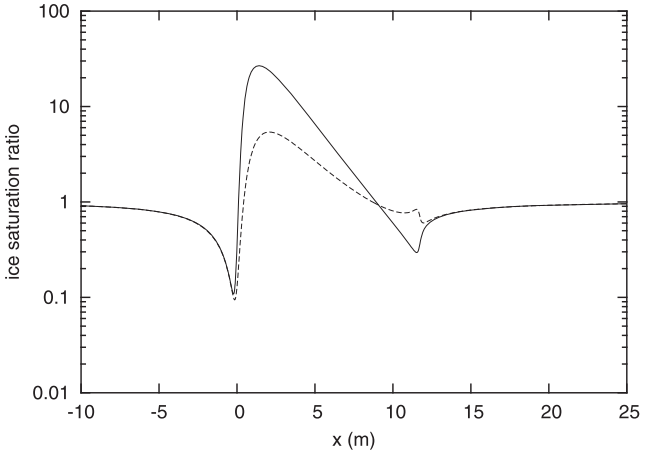

FIG. 7. As in Fig. 6, but for a pair of streamlines that encounter the leading edge of the wing at a vertical distance of 45 cm below (dashed line) and 45 cm above (solid line). Note that the curves are close to each other at the frontal stagnation point but far apart on the wing, with much higher supersaturation on the upper than the lower surface.

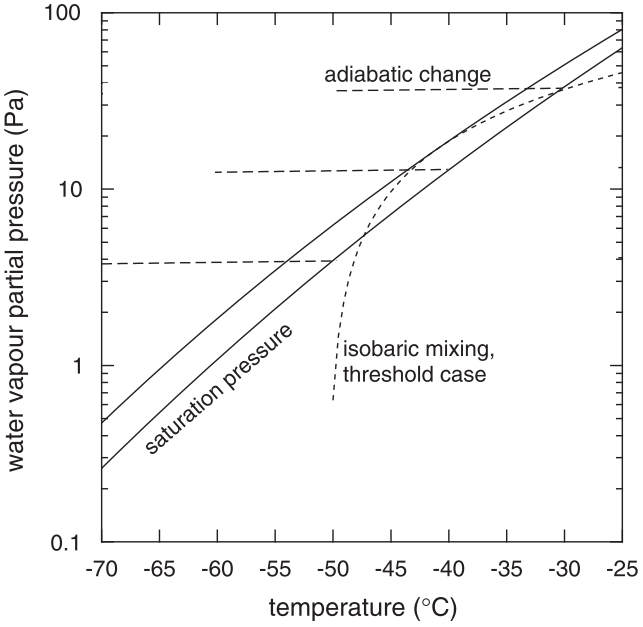

FIG. 8. A T – log e phase diagram showing saturation lines for water and ice, together with some sample adiabatic lines and the critical mixing trajectory for exhaust contrail formation according to the Schmidt–Appleman theory. In this frame the adiabatic lines are straight lines with constant distance, but the saturation curves are slightly concave.

wing's lower surface should therefore be even more so, which probably renders them invisible in front of the bright background posed by the wing's underside.

A ground observer will rarely have a chance to watch an aerodynamic contrail of a high-flying aircraft. The enhanced Rayleigh scattering diminishes the contrast between the contrail and the clear sky more for a ground observer than for an observer in an aircraft close below. In addition, the angular size of the phenomenon is small when seen from the ground, making it difficult both to distinguish the series of the colors and to distinguish an aerodynamic from an exhaust contrail. In our particular example, the colors appeared along 200 m of the contrail, which translates to only about a 1° viewing angle when observed from the ground, compared to 10° when observed from the aircraft only 1 km below. More details are provided in Kärcher et al. (2009).

Let us consider the thermodynamics of aerodynamic condensation. Figure 8 shows a T–log e diagram (i.e., with temperature, T, versus log water vapor partial pressure, log e) including the two saturation curves for liquid water and ice. It also shows the threshold mixing line for jet exhaust contrails for an ambient pressure of 250 hPa. Exhaust contrail formation is possible when the ambient temperature (at a given ambient water partial pressure) is lower than the temperature on the threshold line, whose exact slope (in a linear diagram it is a straight line) depends on aircraft and fuel characteristics. Exhaust contrails are persistent when the phase point of the ambient air is in the area between the two saturation curves (i.e., ice supersaturation; water supersaturation is considered improbable). There are additionally three adiabats plotted in the diagram, referring to different temperatures at ice saturation. Because the flow around an airfoil is nearly adiabatic, the phase change in the flow is along these lines. The figure shows that the highest saturation ratio for a given temperature change is reached in the coldest case (because the saturation curves are slightly concave whereas the adiabats are exactly straight). However, the difference between ambient vapor pressure and ice saturation vapor pressure increases (for a given ambient saturation ratio) with increasing temperature. Hence, crystal growth, which is driven by this difference, will proceed faster at warmer than at colder temperatures, which might lead not only to larger crystals but also to larger total ice mass and optical thickness. So we may expect that aerodynamic condensation leads to stronger effects in warmer air (i.e., at lower altitudes) than higher up in the atmosphere. In particular, strong aerodynamic condensation is possible when jet exhaust contrails are not yet possible because it is still too warm. This is what we have already seen in Fig. 1. However, we expect that the temperatures have to be sufficiently low that during the transient cooling temperatures less than about 235 K will be reached in a certain volume above the wing. This is the temperature below which pure water droplets will freeze spontaneously. Otherwise it is questionable whether freezing of the condensed droplets will occur.

At warmer temperatures it usually needs appropriate (and rare) ice nuclei to let a droplet freeze. When there is no freezing, condensation will probably be followed by evaporation immediately behind the wing, unless the air is supersaturated with respect to water. In the latter case there would be natural clouds already present, so an aerodynamic water contrail would hardly be visible. Only if enough droplets freeze does ice saturation suffice to let an aerodynamic contrail appear and persist in otherwise clear air.

It turned out that supersaturation can be very high in the aerodynamic flow past a wing profile. Accordingly, the driving force for ice crystals once they are formed is unusually large compared with the normal situation found in cirrus clouds, for instance. Cooling/heating rates and rates of pressure changes are extreme, so the microphysics should be subject to the dynamics over the wings. Under such conditions it might be expected that the growth of ice crystals is different from its usual character in tropospheric clouds. The very large driving force implies a very short time scale for diffusion or kinetically limited flow of water molecules from the vapor phase to the particle surface. Surface impedances should become unimportant for crystal growth because the direct flux to the steps and ledges should be sufficient to render surface diffusion unnecessary for advancing the steps. Furthermore, the nucleation of new steps (two-dimensional nucleation) can be expected to be fast because of the large flux of water molecules onto the crystal surface. If the time scale for two-dimensional nucleation is shorter than that of step advancing, many steps should exist simultaneously. This could increase the crystal growth rate. However, it is conceivable that crystal growth under such conditions is so fast that there is not sufficient time to produce an ordered crystal lattice. Even large impurity molecules could be buried by water molecules under these conditions. So the crystallographic character of the growing ice particles may be vastly different (at least transiently) from that of ordinarily grown ice crystals in cirrus clouds. In particular, their surface energies could be larger than that of hexagonal ice (Ih) usually present in the troposphere, so that additionally the equilibrium vapor pressure over such particles could be higher than that of Ih. If this is the case, aerodynamic ice contrails could only survive at a certain ice supersaturation in the ambient air; at lower supersaturations and at saturation they would quickly disappear.

5. Conclusions

In the present paper we have investigated a phenomenon of condensation induced by aircraft, namely the formation of ice due to the cooling in the airflow over the wings while cruising in the upper troposphere. This phenomenon has been known to exist for decades (cf. Rhode and Pearson 1942) yet has been rarely observed although simple thermodynamic arguments suggest that it should often occur. For a more detailed investigation we employed a relatively simple method to compute the flow field around a wing profile. Our method invokes two-dimensionality, frictionless flow, and a slim profile. However, we do not assume an incompressible flow; the usual flight speeds of about Ma = 0.8 do not allow such a simplification. For a number of streamlines we compute pressures, temperatures, and saturation ratios. The former two quantities will be used for microphysics and optics calculations in the companion paper. Here we considered a case study to illustrate with an example how the flow field is perturbed by a wing of an airliner. It was found that the deviations of the thermodynamic properties of the air from their ambient values are quite substantial. For instance, the average pressure difference between the flows underneath and above the wing of a commercial aircraft is about 50 hPa, a substantial fraction of the ambient pressure in the upper troposphere. The temperature and saturation ratio experience vigorous changes on a time scale of milliseconds as well. Such exotic conditions might lead to unusual physical behavior of crystal growth.

The wing depth turned out to be a scaling parameter not only for the flow field but also for the temperature and saturation ratio fields. This means that the effect is strongest for large wing depths, consistent with observations.

Aerodynamic contrail formation is independent of exhaust contrail formation. Whereas exhaust contrails need cold conditions to form, aerodynamic contrails probably form under warmer conditions, as long as the temperature drop over the wing is sufficient to let the condensed droplets freeze. In this sense, aerodynamic and exhaust contrails may be complementary forms of contrails.

Acknowledgments. This work was carried out within the DLR-projects PAZI-2 and CATS. We thank Jeff Well for allowing us to use his photographs for the paper and Frank Holzäpfel for checking a preliminary version of the paper. We are grateful to Ralf Rudnik for providing us with valuable information about wings and their aerodynamics.

REFERENCES

Appleman, H., 1953: The formation of exhaust condensation trails by jet aircraft. *Bull. Amer. Meteor. Soc.,* **34,** 14–20.

Boucher, O., 1999: Air traffic may increase cirrus cloudiness. *Nature,* **397,** 30–31.

Kärcher, B., B. Mayer, K. Gierens, U. Burkhardt, H. Mannstein, and R. Chatterjee, 2009: Aerodynamic contrails: Microphysics and optical properties. *J. Atmos. Sci.,* **66,** 227–243.

Kuhn, P., 1970: Airborne observations of contrail effects on the thermal radiation budget. *J. Atmos. Sci.,* **27,** 937–942.

Landau, L., and E. Lifshitz, 1987: *Course of Theoretical Physics*. 2nd ed. Vol. 6, *Fluid Mechanics,* Butterworth-Heinemann, 539 pp.

Mannstein, H., and U. Schumann, 2005: Aircraft induced contrail cirrus over Europe. *Meteor. Z.,* **14,** 549–554.

Marti, J., and K. Mauersberger, 1993: A survey and new measurements of ice vapor pressure at temperatures between 170 and 250 K. *Geophys. Res. Lett.,* **20,** 363–366.

Minnis, P., D. Young, L. Nguyen, D. Garber, and W. Smith Jr., R. Palikonda, 1998: Transformation of contrails into cirrus clouds during SUCCESS. *Geophys. Res. Lett.,* **25,** 1157–1160.

Penner, J., D. Lister, D. Griggs, D. Dokken, and M. McFarland, 1999: *Aviation and the Global Atmosphere*. Cambridge University Press, 373 pp.

Press, W., B. Flannery, S. Teukolsky, and W. Vetterling, 1989: *Numerical Recipes: The Art of Scientific Computing*. Cambridge University Press, 702 pp.

Rangno, A., and P. Hobbs, 1983: Production of ice particles in clouds due to aircraft penetration. *J. Climate Appl. Meteor.,* **22,** 214–232.

——, and ——, 1984: Further observations of the production of ice particles in clouds by aircraft. *J. Climate Appl. Meteor.,* **23,** 985–987.

Rhode, R., and H. Pearson, 1942: Condensation trails—Where they occur and what can be done about them. National Advisory Committee for Aeronautics Wartime Rep. NACA-WR-L-474, 11 pp.

Sassen, K., 1991: Aircraft-produced ice particles in a highly supercooled altocumulus cloud. *J. Appl. Meteor.,* **30,** 765–775.

Schmidt, E., 1941: Die Entstehung von Eisnebel aus den Auspuffgasen von Flugmotoren. *Schr. Dtsch. Akad. Luftfahrt.,* **44,** 1–15.

Schumann, U., 1994: On the effect of emissions from aircraft engines on the state of the atmosphere. *Ann. Geophys.,* **12,** 365–384.

——, 1996: On conditions for contrail formation from aircraft exhausts. *Meteor. Z.,* **5,** 4–23.

Stordal, F., G. Myhre, E. Stordal, W. Rossow, D. Lee, D. Arlander, and T. Svendby, 2005: Is there a trend in cirrus cloud cover due to aircraft traffic? *Atmos. Chem. Phys.,* **5,** 2155–2162.

Stubenrauch, C., and U. Schumann, 2005: Impact of air traffic on cirrus coverage. *Geophys. Res. Lett.,* **32,** L14813, doi:10.1029/2005GL022707.

Vonnegut, B., 1986: Nucleation of ice crystals in supercooled clouds caused by passage of an airplane. *J. Climate Appl. Meteor.,* **25,** 98.

Zerefos, C., K. Eleftheratos, D. Balis, P. Zanis, G. Tselioudis, and C. Meleti, 2003: Evidence of impact of aviation on cirrus cloud formation. *Atmos. Chem. Phys.,* **3,** 1633–1644.

Zierep, J., 1976: *Theoretische Gasdynamik*. G. Braun, 506 pp.